Ceramics International 49 (2023) 21530–21537

Contents lists available at ScienceDirect

Ceramics International

journal homepage: www.elsevier.com/locate/ceramint

Microstructure-dependent magnetic permeability in ferrites from nanoparticles

A. Barba-Juan [a,b], N. Vicente [a,b], A. Mormeneo-Segarra [a,b], C. Clausell-Terol [a,b,*]

[a] Departamento de Ingeniería Química, Universitat Jaume I, 12071, Castellón, Spain
[b] Instituto Universitario de Tecnología Cerámica, Universitat Jaume I, 12071, Castellón, Spain

ARTICLE INFO

Handling Editor: Dr P. Vincenzini

Keywords:
Complex magnetic permeability
Domain-wall motion
Magnetizing mechanism
Microstructure
NiZn ferrites
Spin rotation

ABSTRACT

Ferrite samples of composition $Cu_{0.12}Ni_{0.23}Zn_{0.65}(Fe_2O_4)$ have been prepared by a conventional ceramic process using different sintering temperatures and dwell times. The average particle size is around 25–30 nm and, after sintering, the average grain size increases to 0.2–5 μm and the relative density is between 88 and 95 % of the theoretical density.

This paper shows that the mathematical model previously tested on ferrite microparticles with the same composition, is also capable to fit the measured complex magnetic permeability-imaginary part (μ'') and to explain why this magnetic property decreases when the particle size of the starting powder changes from micro to nano size. The model confirms the dependence of the magnetizing mechanisms (spin rotation and domain-wall motion) on the two microstructural parameters: average grain size (G) and relative density (ϕ) of the sintered body.

1. Introduction

One of the challenges of today's society is the suppression of electromagnetic interference (EMI) generated by new technologies, which may interfere with the operation of the electrical/electronic devices. Ferrites are one of the most relevant materials used as electromagnetic wave absorbers due to their good chemical stability, high resistivity, excellent electromagnetic properties and cost-effectiveness [1,2]. NiZn ferrites are very useful and efficient (especially when Cu-doped) in the high MHz angular frequency band [3] while MnZn ferrites are limited to the low MHz angular frequency region or at most, high kHz angular frequency band. Cu doping of NiZn ferrites enhances densification and magnetic properties, such as complex magnetic permeability-imaginary part, allowing for outstanding EMI suppression [4–13].

The magnetic properties of bulk ferrites not only depend on their chemical composition, but are also highly dependent on their microstructure (mainly grain size and porosity) [3–6,10,14–17] which is determined in turn by process variables such as shaping and sintering conditions.

In recent years, nanomaterials (particle size less than 100 nm) have been pointed out as a good solution for a large number of applications, since their high specific surface area improves the final properties of the product. However, this is not the case when bulk Cu-doped NiZn ferrites are manufactured to act as electromagnetic wave absorbers. The magnetic properties of ferrite nanocrystals depend on the microstructure and cation distribution. Variation of the microstructure will lead to cation redistribution, which further affects the magnetic properties of the ferrite nanocrystals. Although ferrite nanocrystals exhibit excellent magnetic properties with higher saturation magnetization than microcrystalline ferrites, due to their small particle size and surface effects, saturation magnetization values for bulk ferrite from nanoparticles are lower than for bulk ferrite from microparticles [18]. The grain size reduction induces competition between the strength of the A-A or A-B interaction (either ferromagnetic or antiferromagnetic), arising from Fe clustering at the A or B site, where A refers to tetrahedral sites and B to octahedral sites in spinel structure. Besides, in nanoparticles, a non-negligible fraction of atoms lies on the surface that affects the magnetic properties of the entire system. Surface atoms have a lower coordination number and the nature of the exchange bond determines the increase or decrease in magnetization. They exhibit very interesting magnetic properties at such low grain sizes compared to bulk. Among the main reasons for their magnetization enhancement are cation site exchange between tetrahedral (A) and octahedral (B) sites, shell contribution, non-stoichiometry, mixed valency, impurity phases, spin

* Corresponding author. Departamento de Ingeniería Química, Universitat Jaume I, 12071, Castellón, Spain.
E-mail address: cclausel@uji.es (C. Clausell-Terol).

https://doi.org/10.1016/j.ceramint.2023.03.287
Received 27 January 2023; Received in revised form 16 March 2023; Accepted 29 March 2023
Available online 3 April 2023

canting, strain induced anisotropy and controlled grain boundary. In nanoparticles, the cation distribution profile by itself is not enough to determine the anomalous properties in magnetization and electrical studies, since surface effects become extremely important as the surface-to-volume ratio increases with the particle size reduction. Therefore, surface properties and cation exchange are important issues and have lately become more fundamental when it comes to technological applications [18–20].

Many recent research has been reported showing improvement in the magnetic properties of ferrites nanoparticles, but very few results are found on the magnetic properties of the corresponding sintered bodies [18–37]. Therefore, in this study, bulk Cu-doped NiZn ferrites have been obtained from nanoparticles, showing slightly lower magnetic properties than those obtained from microparticles, as reported by other researchers [20,38].

Complex magnetic permeability (μ(ω)) is the key property used to characterize the ability of ferrites to act as electromagnetic wave absorbers. It represents the material response when an alternating current (AC) magnetic field (H) of angular frequency (ω) is applied to. The real part (μ'(ω)) represents the material storage capacity of the magnetic field, while the imaginary part (μ''(ω)) represents the losses and power dissipation. Moreover, in polycrystalline ferrites the magnetizing mechanisms, known as spin rotation and domain-wall motion, are the two contribution to both the real and imaginary parts [4–6].

Different authors have proposed mathematical models [2,3,12,13,39–49] that are capable of accurately calculating and reproducing frequency dispersion. These models have only been tested on ferrites obtained from microparticles and do not consider the influence of the microstructure.

We have previously reported [4–6] that the complex magnetic permeability of micron-sized ferrites varies with angular frequency, consistent with the extended model proposed by Nakamura [45,49], and is highly dependent on the microstructure through grain size and relative density (or porosity). The influence of the microstructure was introduced in Nakamura model considering the relationship proposed by Pankert [50] and adequately modified by introducing the densification parameter. The final model that we have proposed and tested also includes both magnetizing mechanisms: spin rotation and domain-wall motion [6].

We have also established the following equation to predict the complex magnetic permeability-imaginary part (μ'') in ferrites bodies, obtained by ceramic processing of micrometer-sized powders [5], which were tested at different angular frequencies (ω):

$$\mu''(\omega) = \mu''_S(\omega)\cdot\psi + \mu''_{DW}(\omega)\cdot\left[\frac{G^2}{b''(\omega)+G^2}\right]\cdot\psi \quad (1)$$

where μ''_S is the imaginary part-complex magnetic permeability spin rotation contribution and μ''_{DW} is the imaginary part-complex magnetic permeability domain-wall motion contribution (both are intrinsic values for a specific ferrite chemical composition at a given angular frequency); G is the average grain size and ψ is the densification defined from relative density (ϕ), which, in turn, is the quotient between the apparent density and the theoretical density, as:

$$\psi = \frac{\phi - \phi_{lim}}{1 - \phi_{lim}} \quad (2)$$

ψ is an effective concept when comparing systems of different initial porosities and ϕ_{lim} is the lowest relative density value beyond which the selected magnetic property is clearly measurable, considering the accuracy of the measurement (for lower relative densities the magnetic permeability is virtually zero), being an empirical parameter.

In Eq. (1) b'' is defined as follows:

$$b''(\omega) = 4\cdot\pi^2\cdot d_w^2(\omega) \quad (3)$$

where d_w is the domain-wall width [50].

Eq. (1) states that the contribution of domain-wall motion to magnetic permeability is highly dependent on relative density (ϕ) and average grain size (G), while the contribution of spin rotation it only depends on the relative density (ϕ).

In the aforementioned work [5], it was shown that Eq. (1) is capable of accurately predicting the values of complex magnetic permeability-imaginary part over a wide range of angular frequencies, but particularly at 10^7 Hz where the studied ferrite has the maximum wave absorption. At this frequency, both spin rotation and domain-wall motion mechanisms influence magnetic permeability, leading to an important role of the polycrystalline ferrite microstructure in the magnetic permeability [45]. Eq. (1) was also successfully tested for grain sizes and relative densities ranging, respectively, between 3 and 25 μm and between 0.80 and 0.96.

The main objective of this paper is the validation of Eq. (1) when ferrite specimens are made from a nanoparticle starting powder, in order to:

i. Accurately predict the complex magnetic permeability-imaginary part (μ'') values at an angular frequency of 10^7 Hz
ii. Explain the decrease in magnetic permeability when the particle size of the ferrite starting powder also decreases from micrometer to nanometer scale.

2. Experimental procedure

2.1. Obtaining a nanometric ferrite powder by high-energy milling

The experimental procedure is explained in detail in a previous publication [51]. Briefly, a polycrystalline CuNiZn ferrite powder of chemical composition ($Cu_{0.12}Ni_{0.23}Zn_{0.65}$)$Fe_2O_4$, supplied as pellets by Fair-Rite Products Corp., was used as raw material. The true density of the ferrite powder was experimentally determined in a helium pycnometer (5380 kg/m^3). The pellets were previously ground for 2 h in a FRITSCH Pulverisette 5 planetary ball mill. Disk rotation speed was 260 rpm and milling was carried out in carbon steel bowls, using 7–8 mm diameter carbon steel balls. The resulting powder was then wet-milled in a VMA-GETZMANN Dispermat SL-012 laboratory horizontal bead mill for 48 h (milling speed 4500 rpm). Milling was performed using distilled water and 0.5–0.7 mm diameter zirconia balls. The balls-to-ferrite powder volume ratio was 3:2. A 3 wt % ammonium polymethacrylate solution (DARVAN® C, RT Vanderbilt Company Inc.) was used as dispersing agent.

The milled powder was dried and sieved. Particle/agglomerate-size distribution was determined by laser light diffraction (LLD) (wet method) using a MALVERN Mastersizer 2000 particle size analyzer, as LLD is commonly used to determine particle/agglomerate size (resulting from the physical agglomeration of particles). Particle size has been determined from the BET specific surface area (SBET) measured by nitrogen adsorption in a MICROMERITICS TriStar 3000 instrument. Crystallite size was analyzed by X-ray diffraction (XRD) in a BRUKER D8 Advance diffractometer. Morphological analysis of the particles was performed by scanning electron microscopy (SEM) using a FEI Quanta 200 ESEM FEG microscope. The difference between the XRD and BET results provides a measure of the degree of chemical aggregation of the crystallites. However, only the particle size value is useful in nanopowder processing. In the case of the sample milled for 48 h, an average particle size of about 25–30 nm was achieved [51].

2.2. Shaping, sintering and characterization of ferrite specimens from nanopowders

A brief summary of the experimental procedure reported in previous publications is provided below [14,15]. The milled powders were used to form, by uniaxial dry pressing, cylindrical and toroidal specimens (3 mm thick and 19 mm outer diameter; 6 mm inner diameter for toroidal

specimens). The samples were air sintered in an electric laboratory furnace. Bulk density was determined by the Archimedes method and the relative density of each specimen was calculated as the quotient between the bulk density and the theoretical density. Average grain size was determined from the grain size distribution using an image analysis of the cross-sectional area of the rectangular thermal etched surface of each specimen using scanning electron microscopy (SEM). The real and the imaginary part of the complex magnetic permeability were determined on an Agilent E4991A RF impedance/material analyzer over a frequency range of 10 MHz–1000 MHz using an Agilent 16454A magnetic material test fixture.

Samples were shaped at 150 MPa compaction pressure and sintered at different maximum temperatures (1000, 1050, 1100 and 1200 °C) and different dwell times (1, 3, 5, 10, 15, 20 and 25 min), which led to different final microstructures of the studied ferrite. The heating rate was 12 °C/min, with a 2-h stop at 500 °C to remove the organic compounds used to shape the green bodies. The cooling rate used was 20 °C/min. Table 1 shows the values of P (pressing pressure), T (maximum sintering temperature) and t (sintering dwell time at maximum temperature) used in the 28 experiments that have allowed obtaining a wide range of relative densities and average grain sizes.

Experimental values of ϕ (whose relative error is always lower than 1%), G, S (width of the grain size distribution) and μ'' (magnetic complex permeability-imaginary part at 10^7 Hz) for each specimen are also shown in Table 1. G and S were determined using image analysis of the cross-sectional area of the rectangular thermally etched surface of each cylindrical sintered specimen, observed using SEM. Specimens were thermally-etched in air at a temperature 100–120 °C lower than their sintering temperature, for 1 h and at a heating rate of 15 °C/min. S was defined as G_{90}-G_{10}, where G_{90} and G_{10} are those diameters below which 90 and 10 vol% of total particles lie, respectively, based on the accumulated grain size distribution curve. The grain size distribution of all samples is monomodal and relatively narrow, although they broadened with increasing both sintering time and temperature.

Scanning electron micrographs of polished and etched cross-sectional surfaces of all samples do not show any kind of precipitated phases at the grain boundaries (such as the crystalline zinc or copper phases found under certain sintering conditions in previous studies [7,8,52,53]), suggesting that the chemical composition of the grains has remained constant throughout the sintering process in the 28 samples studied. It has also been verified that the X-ray diffraction is the same for all the samples, as well as for the starting powder (Ni–Zn spinel).

Table 1
Processing conditions and sintered microstructural properties of the Cu-doped NiZn-polycrystalline ferrite specimens.

P (MPa)	T (°C)	t (min)	ϕ	ψ	G_{50} (μm)	S (μm)	μ"
150	1000	1	0.878	0.060	0.303	0.213	15.13
		3	0.878	0.061	0.304	0.257	20.89
		5	0.879	0.068	0.262	0.217	23.20
		10	0.892	0.170	0.289	0.218	53.53
		15	0.893	0.179	0.308	0.226	76.74
		20	0.896	0.201	0.364	0.395	99.45
		25	0.902	0.243	0.393	0.344	119.02
	1050	1	0.918	0.369	0.540	0.454	225.74
		3	0.918	0.370	0.517	0.489	228.91
		5	0.922	0.400	0.506	0.456	231.65
		10	0.925	0.420	0.563	0.389	254.74
		15	0.926	0.433	0.553	0.444	270.91
		20	0.931	0.468	0.507	0.430	259.10
		25	0.929	0.451	0.606	0.447	281.63
	1100	1	0.935	0.501	0.847	1.257	272.82
		3	0.940	0.542	0.654	0.809	280.78
		5	0.939	0.528	1.192	1.195	284.19
		10	0.941	0.549	1.048	1.372	300.68
		15	0.940	0.541	0.885	1.271	313.76
		20	0.943	0.565	1.387	1.171	316.07
		25	0.943	0.559	1.210	1.126	327.62
	1200	1	0.938	0.523	4.401	5.575	350.41
		3	0.944	0.572	4.421	5.788	358.88
		5	0.946	0.584	4.377	6.123	342.40
		10	0.947	0.590	3.979	5.559	361.15
		15	0.948	0.596	3.955	5.369	356.47
		20	0.947	0.594	3.581	5.606	369.87
		25	0.945	0.579	4.859	5.298	360.45

2.3. A matter of nomenclature

The ferrite specimens obtained by sintering a micrometric ferrite starting powder will hereinafter be referred to as ***microferrite***. The average grain size of the sintered samples ranges from 3 to 25 μm [4–6]. This microferrite is used to compare the results obtained in present study.

The ferrite specimens obtained by sintering a nanometric ferrite starting powder will hereinafter be referred to as ***nanoferrite***, although the average grain size of the sintered samples ranges from 0.2 to 5 μm, as indicated in the next section.

3. Results and discussion

Fig. 1 shows the microstructure of some sintered specimens at different sintering temperatures and dwell times. It can be clearly seen that the grain size increases with the sintering temperature and with the dwell time, for a constant sintering temperature and residence time, respectively. The most notable fact is that although average particle size of the starting powder is around 25–30 nm, the average grain size of the sintered ferrite specimens is in the micrometer range. Therefore, it would actually be more accurate to speak of micro-sized ferrites obtained from nanoparticles. In any case, the average grain size of the sintered ferrite is always less than 5 μm, while from micrometric powders average grain sizes of up to 25 μm are reached [4].

Fig. 2 depicts the experimental values of μ" vs. G from Table 1, for the 28 specimens tested. It should be highlighted:

i. The average grain size of the sintered specimens (G) is always below 5 μm, due to the small particle size of the nanometric starting powder (around 25–30 nm).
ii. The greater the average grain size, the higher the value of μ'', which tends asymptotically to approximately 350.

However, a similar study carried out with the same ferrite composition but using a micrometric starting powder (around 0.5 μm) stated that the average grain size of the sintered specimens (G) was always below 25 μm and the value of μ'' tended asymptotically to approximately 550 (values clearly higher than the values reported in this work) [5].

The discrete points in Fig. 2 correspond to the experimental values of the nanoferrite samples. The solid line corresponds to the calculated values of μ'' from Eq. (1) using the same parameters previously determined for the same ferrite composition at 10^7 Hz (ϕ_{lim}, = 0.65, $\mu''_S = 291$, $\mu''_{DW} = 324$ and $d_w = 185$ nm) [6] and the empirical relationship between ϕ and G ($\phi = 0.915 \cdot \left[G^{1.833}/\left(0.408 + G^{1.819}\right)\right]$), obtained with the microferrite material, with an average particle size of about 0.5 μm. In this case, it can be observed that the theoretical curve does not accurately reproduce the experimental data.

This observed difference between the sintered nanoferrrite and microferrite specimens (made from nanoparticles and microparticles, respectively) seems apparently incongruous, but can be explained by assuming that ϕ_{lim} in Eq. (2) and domain-wall thickness (d_w) in Eq. (3) are highly dependent on the green body microstructure of the specimens and, therefore, on the particle size of the starting powder [50].

The plot of μ'' *vs.* relative density (Fig. 3) allows estimating a value of ϕ_{lim} around 0.87. This relative density limit value depends not only on the sintering conditions but also on the green body microstructure, which is determined by the particle size distribution of the raw material

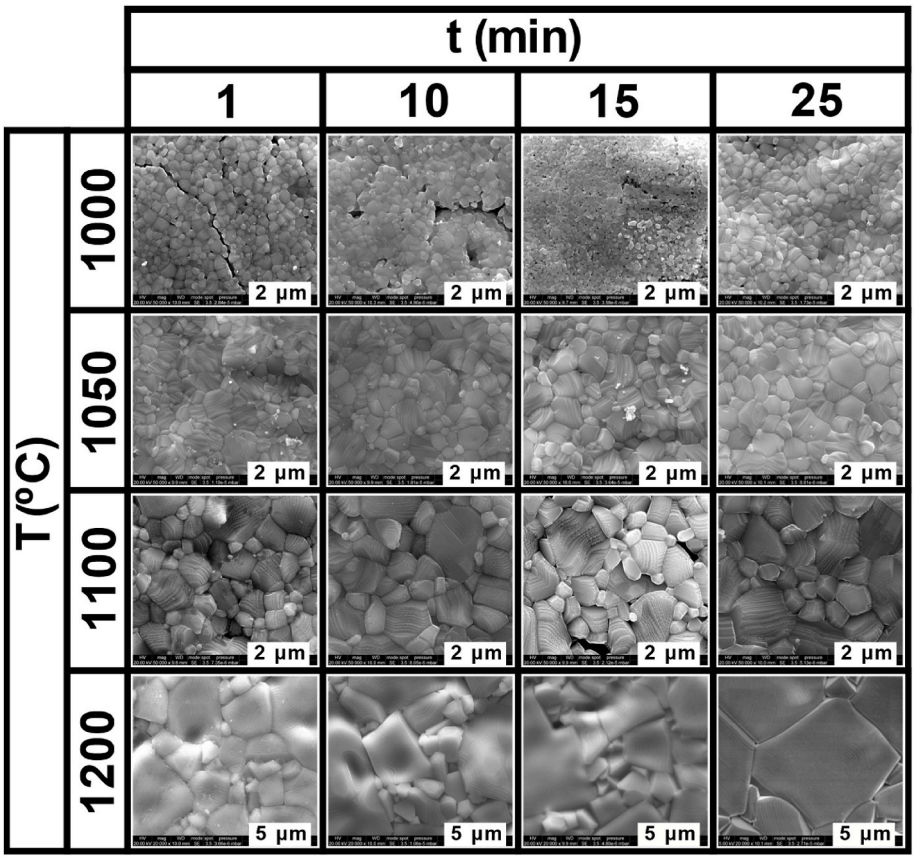

Fig. 1. SEM micrograph of CuNiZn microferrite samples sintered at different sintering temperatures and dwell times.

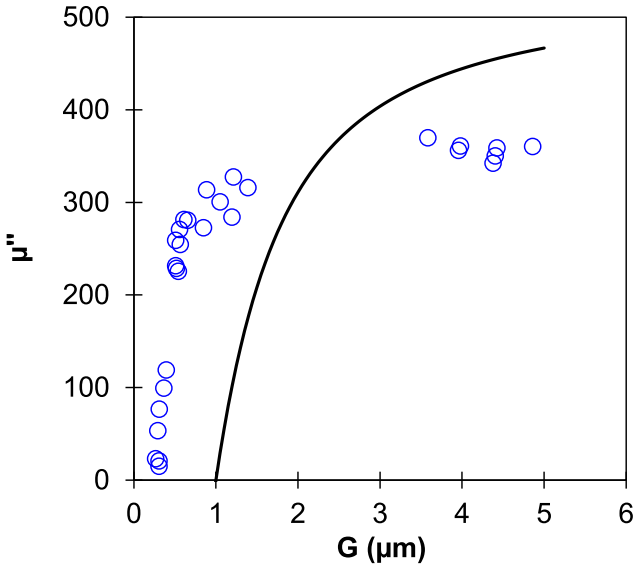

Fig. 2. Nanoferrite experimental data (discrete points) and calculated values using Eq. (1) (solid line) of complex magnetic permeability – imaginary part *vs.* average grain size.

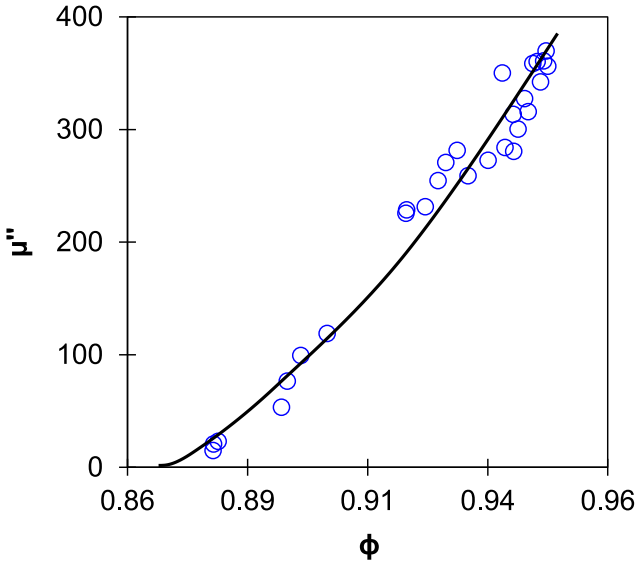

Fig. 3. Graphical estimation of ϕ_{lim}.

and the shaping conditions (dry uniaxial pressing pressure).

Although the green body microstructure is difficult to described, it is usually characterized by the grain and pore size distributions and their corresponding mean diameters. The literature on ceramic processing states [54–56] that the larger the size of the powder particles, the higher the apparent density of ceramic body shaped by powder pressing, keeping the pressing conditions constant. Therefore, microsized powders lead to denser (less porous) ferrite green bodies than nanosized powders. Furthermore, average pore size will be larger in microferrite green bodies than in nanoferrite ones. Table 2 summarizes this reasoning for better understanding.

The microstructure of sintered bodies is highly dependent on the microstructure of the green bodies, and the final microstructure is reminiscent of the green body microstructure: the same patterns are

Table 2
Relative values of some microstructural parameters of microsized versus nanosized ferrite bodies (for constant shaping conditions).

PARTICLES		GREEN BODIES			SINTERED BODIES				
Size	Particle size	Relative density	Porosity	Pore size	Relative density	Porosity	Pore size	Grain boundary	Magnetic wall domains
Micrometric	↑	↑	↓	↑	↑	↓	↑	High continuity	Large
Nanometric	↓	↓	↑	↓	↓	↑	↓	Low continuity	Small

replicated during sintering (see Table 2). The presence of a large number of small pores in the nanoferrite *versus a* few large pores in the microferrite can produce a discontinuous and highly fragmented overall grain boundary. By contrast, the total grain boundary in the microferrite will be virtually continuous, interrupted only by a few large pores. Consequently, microferrite will have large wall domains, while nanoferrite will have very small ones. Usually, the higher the angular frequency, the lower the influence of the domain-wall motion mechanism [44,45,47,49], although at the studied angular frequency of 10^7 Hz, the contribution of the magnetic domain-wall motion to complex magnetic permeability – imaginary part has a similar weight to that of the spin rotation contribution [6], and the magnetic behavior of nanoferrite worsens compared to the magnetic behavior of the microferrite.

Nanoferrite powder processing increases ϕ_{lim} because it is difficult to achieve a high bulk density to ensure high grain boundary values. The microstructure of the sintered bodies is suitable to show good magnetic properties only when the relative density reaches values close to 0.87 or higher (Fig. 3). According to Eq. (2), only these high values of ϕ_{lim} allow high values of ψ, which also requires reaching very high values of ϕ (extremely difficult when processing nanosized powders).

Summarizing, ferrite nanoparticles may have better electromagnetic properties than microparticles, but when the specimens are shaped and sintered, the exact opposite occurs for two fundamental reasons:

i. The difficulty of reaching high values of ϕ (higher than 0.96) makes it difficult to get high densification values (ψ), despite the high value of ϕ_{lim}.
ii. The presence in both cases of a large grain boundary, but extremely discontinuous in the nanoferrites because the porosity comprises a large number of very small pores.

This can therefore explain the electromagnetic behavior of many $MFeO_4$ nanoferrites and the dilemmas reported in literature [18,19].

Fig. 2 also shows that μ'' tends asymptotically to approximately 350, while the reported value for the microsized ferrite was around 550 [5]. This notable difference is also based on the increased number of grain boundaries when processing ferrite nanopowders.

Furthermore, Fig. 4 shows how permeability increases rapidly and linearly when the average grain size is less than 1 μm due to being in the monodomain region [16,57–66]. However, when this grain size is exceeded, the permeability reaches a saturation value of about 350, much lower than the 550 reached in microferrite.

Since the domain-wall thickness d_w in Eq. (3) is also highly dependent on the green body microstructure of the specimens and, therefore, on the particle size of the starting powder [50], the parameter b'' must also be modified, since increasing the number of grain boundaries leads to decreased domain-wall thickness and magnetic permeability, according to Pankert [50].

Therefore, based on the above considerations, Eq. (1) can be written as follows:

$$\mu'' = 291 \cdot \psi + 324 \cdot \left(\frac{G^2}{b''(\omega) + G^2}\right) \cdot \psi \tag{4}$$

$$\mu'' = \left[291 + 324 \cdot \left(\frac{G^2}{4 \cdot \pi^2 \cdot d_w^2(\omega) + G^2}\right)\right] \cdot \left(\frac{\phi - 0.87}{1 - 0.87}\right) \tag{5}$$

where μ''_S and μ''_{DW} take the previously determined values for the same

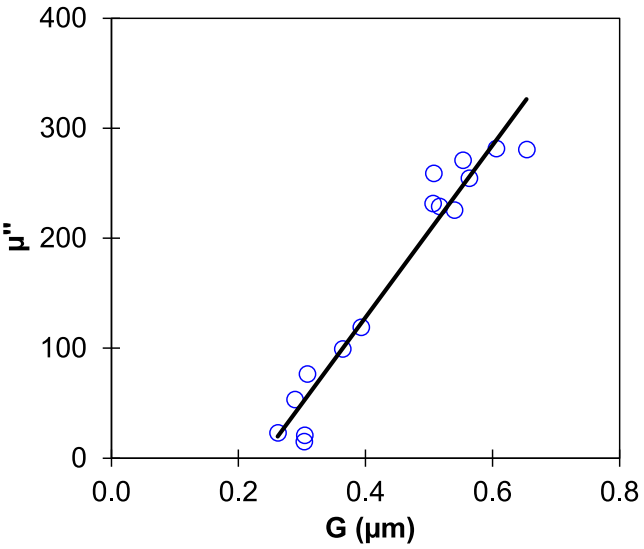

Fig. 4. Influence of average grain size on complex magnetic permeability – imaginary part in nanoferrite.

microferrite (291 and 324, respectively [6], which are intrinsic for this material at the given angular frequency of 10^7 Hz), and $\phi_{lim} = 0.87$.

A nonlinear least-squares method has been used to fit experimental data shown in Table 1 to Eq. (5), allowing the estimation of domain-wall width by minimizing the sum of squared residuals. The estimated value of d_w has been found to be 39 nm ($39 \cdot 10^{-3}$ μm). This figure is smaller than the 185 nm previously obtained for the microferrite [6].

Therefore, Eq. (5) can be rewritten as:

$$\mu'' = \left[291 + 324 \cdot \left(\frac{G^2}{4\pi^2 \cdot \left(39 \cdot 10^{-3}\right)^2 + G^2}\right)\right] \cdot \left(\frac{\phi - 0.87}{1 - 0.87}\right) \tag{6}$$

where G is in μm.

To reproduce experimental data, the following empirical relationship between ϕ and G has been obtained by nonlinear fitting of the respective values shown in Table 1:

$$\phi = 0.954 \cdot \left(\frac{G^{1.407}}{0.015 + G^{1.413}}\right) \tag{7}$$

Therefore, Eq. (1) can be rewritten as:

$$\mu'' = \left[291 + 324 \cdot \left(\frac{G^2}{4 \cdot \pi^2 \cdot 39^2 \bullet 10^6 + G^2}\right)\right] \cdot \left[\frac{0.954 \cdot \left(\frac{G^{1.407}}{0.015 + G^{1.413}}\right) - 0.87}{1 - 0.87}\right] \tag{8}$$

equation that should satisfactorily reproduce the experimental data.

Indeed, Fig. 5 shows the values of μ'' calculated using Eq. (8) (solid line) together with the experimental data (discrete points) for the angular frequency of 10^7 Hz. The mathematical model accurately reproduces the experimental data, as was done with the previously studied microferrite [5,6]. Furthermore, the model also predicts the asymptotic limit to which permeability tends in nanoferrite and explains the

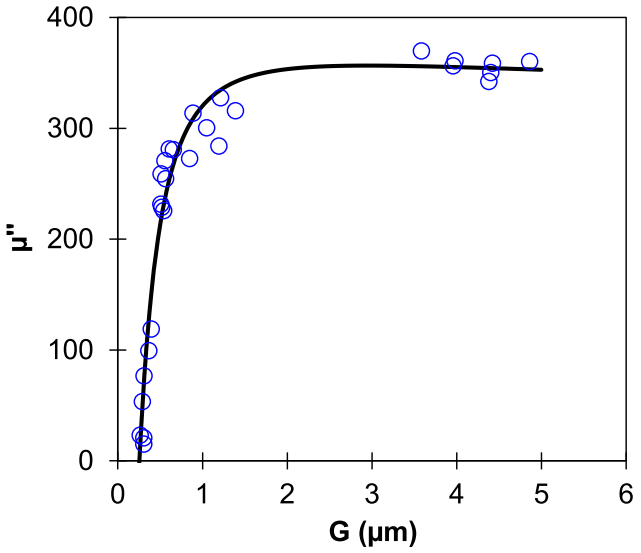

Fig. 5. Experimental (discrete points) and calculated values (solid line) using Eq. (8) of complex magnetic permeability - imaginary part for nanoferrite.

difference with microferrite.

The results obtained confirm the invariance of the intrinsic parameters $\mu''_S(\omega)$ and $\mu''_{DW}(\omega)$ in the proposed model for a given composition at a given angular frequency. Likewise, the model:

i. Explains the worsening of the complex magnetic permeability-imaginary part (μ'') when the processing of ferrite bodies goes from using microparticles to nanoparticles; the limit or saturation value of μ'' decreases 1.5 times (from 550 to 350).
ii. Provides accurate μ'' values from average grain size and relative density of sintered body.

4. Conclusions

Literature reports that nanoparticles of NiZn ferrites have better electromagnetic behavior than microparticles. However, ceramic bodies obtained by shaping and sintering nanopowders have worse behavior than those obtained from micropowders, as stated in this article for complex magnetic permeability-imaginary part (the most important property to characterize an EMI suppressor material). Furthermore, the complex magnetic permeability-imaginary part of nanoferrite increases with relative density and average grain size, but the maximum value achieved is substantially lower ($\mu'' = 350$) than for microferrite ($\mu'' = 550$).

The above facts can be explained using the mathematical model that we have previously developed and tested for microferrite.

When this model has been applied to nanoferrite, the invariance of the intrinsic parameters $\mu''_S(\omega)$ and $\mu''_{DW}(\omega)$ representing the contribution of spin rotation and domain-wall motion mechanisms to the magnetic permeability has been confirmed. That is, both parameters depend solely on the chemical composition, at a given angular frequency, but they are not related to the size of the starting powder or the grain size of the sintered ceramic body.

Similarly, this model requires to determine the relative density limit, which is the lowest relative density value from which the selected magnetic property is clearly measurable, considering measurement accuracy. This relative density limit value depends not only on the sintering conditions but also on the green body microstructure, set by the particle size distribution of the raw material and the shaping conditions. A value of $\phi_{lim} = 0.87$ has been found for nanoferrite, while a lower value is required for microferrite ($\phi_{lim} = 0.65$). The high value of ϕ_{lim} explains the difficulty of obtaining high values of relative density of sintered bodies (ϕ greater than 0.96), making it extremely difficult to reach high values of densification (ψ) and, therefore, reaching a maximum value of μ'' lower than that of microferrite.

This model allows to accurately calculate and predict the values of μ'' for any average grain size and relative density of the sintered nanoferrite body, as reported in the previously studied microferrite.

In conclusion, it can be stated that this model, which relates the complex magnetic permeability-imaginary part with the magnetization mechanisms (spin rotation and domain-wall motion) and with the microstructure of the sintered body (relative density and average grain size), has been validated for and extended from micro to nanoferrite, supporting the hypotheses on which the aforementioned model was based.

Declaration of competing interest

The authors declare that they have no known competing financial interests or personal relationships that could have appeared to influence the work reported in this paper.

Acknowledgment

This research was funded by MCIN/AEI/10.13039/501100011033 and, as appropriate, by ESF Investing in your future, grant numbers MAT2016–76320-R and PID2020-112659RB-100, by the Generalitat Valenciana, grant number ACIF/2021/294 and by the Universitat Jaume I, grant numbers UJIB2017-48, UJIB2020-13 and POSDOC/2020/04. Complex relative permeability determination was carried out at the central facilities (Servei Central d'Instrumentació Científica) of the Universitat Jaume I.

References

[1] A. Goldman, Modern Ferrite Technology, Second Editon, 2006, https://doi.org/10.1017/CBO9781107415324.004.
[2] T. Tsutaoka, Frequency dispersion of complex permeability in Mn-Zn and Ni-Zn spinel ferrites and their composite materials, J. Appl. Phys. 39 (2003) 2789–2796, https://doi.org/10.1063/1.1542651.
[3] H. Su, H. Zhang, X. Tang, Y. Jing, Z. Zhong, Complex permeability and permittivity spectra of polycrystalline Ni-Zn ferrite samples with different microstructures, J. Alloys Compd. 481 (2009) 841–844, https://doi.org/10.1016/j.jallcom.2009.03.133.
[4] A. Barba, C. Clausell, J.C. Jarque, L. Nuño, Magnetic complex permeability (imaginary part) dependence on the microstructure of a Cu-doped Ni–Zn-polycrystalline sintered ferrite, Ceram. Int. 46 (2020) 14558–14566, https://doi.org/10.1016/j.ceramint.2020.02.255.
[5] A. Barba-Juan, N. Vicente, A. Mormeneo-Segarra, C. Clausell-Terol, Influence of microstructure and magnetizing mechanisms on magnetic complex permeability (imaginary part) of a Cu-doped Ni–Zn polycrystalline ferrite, Ceram. Int. 47 (2021) 29504–29508, https://doi.org/10.1016/j.ceramint.2021.07.119.
[6] A. Barba-Juan, A. Mormeneo-Segarra, N. Vicente, J.C. Jarque, C. Clausell-Terol, Frequency dispersion model of the complex permeability of soft ferrites in the microwave frequency range, J. Am. Ceram. Soc. 105 (2022) 2725–2734, https://doi.org/10.1111/jace.18267.
[7] A. Barba, C. Clausell, L. Nuño, J.C.J.C. Jarque, ZnO and CuO crystal precipitation in sintering Cu-doped Ni-Zn ferrites. II. Influence of sintering temperature and sintering time, J. Eur. Ceram. Soc. 37 (2017) 169–177, https://doi.org/10.1016/j.jeurceramsoc.2016.07.033.
[8] A. Barba, C. Clausell, J.C.J.C. Jarque, M. Monzó, ZnO and CuO crystal precipitation in sintering Cu-doped Ni-Zn ferrites. I. Influence of dry relative density and cooling rate, J. Eur. Ceram. Soc. 31 (2011) 2119–2128, https://doi.org/10.1016/j.jeurceramsoc.2011.05.007.
[9] M. Manjurul Haque, M. Huq, M.A. Hakim, Influence of CuO and sintering temperature on the microstructure and magnetic properties of Mg- Cu- Zn ferrites, J. Magn. Magn Mater. 320 (2008) 2792–2799, https://doi.org/10.1016/j.jmmm.2008.06.017.
[10] A.C.F.M. Costa, E. Tortella, M.R. Morelli, R.H.G.A. Kiminami, Synthesis, microstructure and magnetic properties of Ni-Zn ferrites, J. Magn. Magn Mater. 256 (2003), https://doi.org/10.1016/S0304-8853(02)00449-3.
[11] M.F. Huq, D.K. Saha, R. Ahmed, Z.H. Mahmood, Ni-Cu-Zn ferrite research: a brief review, J. Sci. Res. 5 (2013), https://doi.org/10.3329/jsr.v5i2.12434.
[12] O.F. Caltun, L. Spinu, A. Stancu, L.D. Thung, W. Zhou, Study of the microstructure and of the permeability spectra of Ni-Zn-Cu ferrites, J. Magn. Magn Mater. (2002) 242–245, https://doi.org/10.1016/S0304-8853(01)01187-8, 160–162.
[13] K. Kawano, N. Sakurai, S. Kusumi, H. Kishi, Magnetic permeability and microstructure of the Bi,Si oxides-doped NiZnCu ferrite composite material,

J. Magn. Magn Mater. 297 (2006) 26–32, https://doi.org/10.1016/j.jmmm.2005.01.033.
[14] C. Clausell, A. Barba, L. Nuño, J.C. Jarque, Electromagnetic properties of ferrite tile absorber as a function of compaction pressure, Ceram. Int. 42 (2016) 17303–17309, https://doi.org/10.1016/j.ceramint.2016.08.026.
[15] C. Clausell, A. Barba, L. Nuño, J.C. Jarque, Effect of average grain size and sintered relative density on the imaginary part - μ″ of the complex magnetic permeability of $(Cu_{0.12}Ni_{0.23}Zn_{0.65})Fe_2O_4$ system, Ceram. Int. 42 (2016) 4256–4261, https://doi.org/10.1016/j.ceramint.2015.11.101.
[16] K. Kawano, M. Hachiya, Y. Iijima, N. Sato, Y. Mizuno, The grain size effect on the magnetic properties in NiZn ferrite and the quality factor of the inductor, J. Magn. Magn Mater. 32 (2009) 2488–2493, https://doi.org/10.1016/j.jmmm.2009.03.015.
[17] T. Jahanbin, M. Hashim, K. Amin Mantori, Comparative studies on the structure and electromagnetic properties of Ni-Zn ferrites prepared via co-precipitation and conventional ceramic processing routes, J. Magn. Magn Mater. 322 (2010) 2684–2689, https://doi.org/10.1016/j.jmmm.2010.04.008.
[18] W. Wang, Z. Ding, X. Zhao, S. Wu, F. Li, M. Yue, J.P. Liu, Microstructure and magnetic properties of MFe_2O_4 (M = Co, Ni, and Mn) ferrite nanocrystals prepared using colloid mill and hydrothermal method, J. Appl. Phys. 117 (2015), https://doi.org/10.1063/1.4917463, 17A328-1-17A328-4.
[19] A.A. Kumar, Investigation of Electrical and Magnetic Properties of Spinel Nano Ferrites, Pondicherry University, India, 2016.
[20] A. Hajalilou, S.A. Mazlan, A review on preparation techniques for synthesis of nanocrystalline soft magnetic ferrites and investigation on the effects of microstructure features on magnetic properties, Appl. Phys. Mater. Sci. Process 122 (2016) 1–15, https://doi.org/10.1007/S00339-016-0217-2/FIGURES/8.
[21] D. Gherca, A. Pui, V. Nica, O. Caltun, N. Cornei, Eco-environmental synthesis and characterization of nanophase powders of Co, Mg, Mn and Ni ferrites, Ceram. Int. 40 (2014) 9599–9607, https://doi.org/10.1016/j.ceramint.2014.02.036.
[22] S. Burianova, J. Poltierova Vejpravova, P. Holec, J. Plocek, D. Niznansky, Surface spin effects in La-doped $CoFe_2O_4$ nanoparticles prepared by microemulsion route, J. Appl. Phys. 110 (2011), 073902, https://doi.org/10.1063/1.3642992.
[23] A.S. Nikolić, N. Jović, J. Rogan, A. Kremenović, M. Ristić, A. Meden, B. Antić, Carboxylic acids and polyethylene glycol assisted synthesis of nanocrystalline nickel ferrites, Ceram. Int. 39 (2013) 6681–6688, https://doi.org/10.1016/j.ceramint.2013.01.106.
[24] B. Antic, A. Kremenovic, N. Jovic, M.B. Pavlovic, C. Jovalekic, A.S. Nikolic, G. F. Goya, C. Weidenthaler, Magnetization enhancement and cation valences in nonstoichiometric (Mn,Fe) 3-δO 4 nanoparticles, J. Appl. Phys. (2012), 074309, https://doi.org/10.1063/1.3700228.
[25] F. Nakagomi, S.W. Da Silva, V.K. Garg, A.C. Oliveira, P.C. Morais, A. Franco Júnior, E.C.D. Lima, The influence of cobalt population on the structural properties of $Co_x Fe_{3-x} O_4$, J. Appl. Phys. (2007) 09M514, https://doi.org/10.1063/1.2712821.
[26] V. Musat, O. Potecasu, R. Belea, P. Alexandru, Magnetic materials from co-precipitated ferrite nanoparticles, Mater. Sci. Eng. B Solid-State Mater. Adv. Technol. 167 (2010) 85–90, https://doi.org/10.1016/j.mseb.2010.01.038.
[27] M.K. El Nimr, B.M. Moharram, S.A. Saafan, S.T. Assar, Particle size distribution, magnetic permeability and dc conductivity of nano-structured and bulk LiNiZn-ferrite samples, J. Magn. Magn Mater. 322 (2010) 2108–2112, https://doi.org/10.1016/j.jmmm.2010.01.042.
[28] S.A. Saafan, S.T. Assar, B.M. Moharram, M.K. El Nimr, Comparison study of some structural and magnetic properties of nano-structured and bulk Li-Ni-Zn ferrite samples, J. Magn. Magn Mater. 322 (2010), https://doi.org/10.1016/j.jmmm.2009.10.027.
[29] R.B. Kamble, V. Varade, K.P. Ramesh, V. Prasad, Domain size correlated magnetic properties and electrical impedance of size dependent nickel ferrite nanoparticles, AIP Adv. 5 (2015), 017119, https://doi.org/10.1063/1.4906101.
[30] H.S. Kim, D. Kim, B.S. Kwak, G.B. Han, M.H. Um, M. Kang, Synthesis of magnetically separable core at shell structured $NiFe_2O_4$ at TiO_2 nanomaterial and its use for photocatalytic hydrogen production by methanol/water splitting, Chem. Eng. J. 243 (2014) 272–279, https://doi.org/10.1016/j.cej.2013.12.046.
[31] D. Makovec, A. Kodre, I. Arčon, M. Drofenik, Structure of manganese zinc ferrite spinel nanoparticles prepared with co-precipitation in reversed microemulsions, J. Nanoparticle Res. 11 (2009) 1145–1158, https://doi.org/10.1007/s11051-008-9510-0.
[32] D. Makovec, A. Kodre, I. Arčon, M. Drofenik, The structure of compositionally constrained zinc-ferrite spinel nanoparticles, J. Nanoparticle Res. 13 (2011) 1781–1790, https://doi.org/10.1007/s11051-010-9929-y.
[33] S. Gyergyek, D. Makovec, A. Kodre, I. Arčon, M. Jagodič, M. Drofenik, Influence of synthesis method on structural and magnetic properties of cobalt ferrite nanoparticles, J. Nanoparticle Res. 12 (2010) 1263–1273, https://doi.org/10.1007/s11051-009-9833-5.
[34] S. Amiri, H. Shokrollahi, Magnetic and structural properties of RE doped Co-ferrite (RE=Nd, Eu, and Gd) nano-particles synthesized by co-precipitation, J. Magn. Magn Mater. 345 (2013) 18–23, https://doi.org/10.1016/j.jmmm.2013.05.030.
[35] S.R. Naik, A.V. Salker, Change in the magnetostructural properties of rare earth doped cobalt ferrites relative to the magnetic anisotropy, J. Mater. Chem. 22 (2012) 2740–2750, https://doi.org/10.1039/c2jm15228b.
[36] M.A. Gabal, Y.M. Al Angari, H.M. Zaki, Structural, magnetic and electrical characterization of Mg-Ni nano-crystalline ferrites prepared through egg-white precursor, J. Magn. Magn Mater. 363 (2014) 6–12, https://doi.org/10.1016/j.jmmm.2014.03.007.
[37] J. Xiang, Y. Chu, X. Shen, G. Zhou, Y. Guo, Electrospinning preparation, characterization and magnetic properties of cobalt-nickel ferrite $(Co_{1-x}Ni_xFe_2O_4)$ nanofibers, J. Colloid Interface Sci. 376 (2012) 57–61, https://doi.org/10.1016/j.jcis.2012.02.068.
[38] K.A. Korolev, J.S. McCloy, M.N. Afsar, Ferromagnetic resonance of micro- and nano-sized hexagonal ferrite powders at millimeter waves, J. Appl. Phys. 111 (2012), https://doi.org/10.1063/1.3671793.
[39] T. Nakamura, T. Tsutaoka, K. Hatakeyama, Frequency dispersion of permeability in ferrite composite materials, J. Magn. Magn Mater. 138 (1994) 319–328, https://doi.org/10.1016/0304-8853(94)90054-X.
[40] S. Yan, S. Liu, L. He, J. He, S. Huang, L. Deng, Investigation on microstructure and magnetic properties in V_2O_5 doped NiCuZn ferrite, Mater. Res. Express 6 (2019), https://doi.org/10.1088/2053-1591/ab1782.
[41] S. Boggi, W.G. Fano, Numerical response and causality study of the magnetic permeability-frequency function of NiZn ferrites using Genetic Algorithm, J. Magn. Magn Mater. 500 (2020), https://doi.org/10.1016/j.jmmm.2019.166305.
[42] J. Jankovskis, Complex permeability of ferrites correlated with their microstructure, Adv. Sci. Technol. 45 (2006) 2560–2565. https://doi.org/10.4028/www.scientific.net/ast.45.2560.
[43] C.A. Stergiou, V. Zaspalis, Analysis of the complex permeability of NiCuZn ferrites up to 1 GHz with regard to Cu content and sintering temperature, Ceram. Int. 40 (2014) 357–366, https://doi.org/10.1016/j.ceramint.2013.06.010.
[44] N. Ponomarenko, Study of Frequency and Microstructure Dependencies of Magnetic Losses of Ferrite Materials and Components, Riga Technical University, 2014.
[45] T. Nakamura, Study on High-Frequency Permeability in Ferrite Ceramics and Ferrite Composite Materials, Hiroshima University, 1996.
[46] N. Hamilton, The small-signal frequency response of ferrites, High Freq. Electron. June (2011) 36–52.
[47] T. Nakamura, Low-temperature sintering of Ni-Zn-Cu ferrite and its permeability spectra, J. Magn. Magn Mater. 168 (1997) 258–291, https://doi.org/10.1016/S0304-8853(96)00709-3.
[48] W.G. Fano, S. Boggi, A.C. Razzitte, Causality study and numerical response of the magnetic permeability as a function of the frequency of ferrites using Kramers-Kronig relations, Phys. B Condens. Matter 403 (2008) 526–530, https://doi.org/10.1016/j.physb.2007.08.218.
[49] T. Tsutaoka, M. Ueshima, T. Tokunaga, T. Nakamura, K. Hatakeyama, Frequency dispersion and temperature variation of complex permeability of Ni-Zn ferrite composite materials, J. Appl. Phys. 78 (1995) 3983–3991, https://doi.org/10.1063/1.359919.
[50] J. Pankert, Influence of grain boundaries on complex permeability in MnZn ferrites, J. Magn. Magn Mater. 138 (1994) 45–51, https://doi.org/10.1016/0304-8853(94)90397-2.
[51] A. Barba, C. Clausell, J.C. Jarque, M. Monzó, Obtainment of nanoparticulate CuNiZn ferrite powder by high-energy milling, J. Ceram. Soc. Japan. 120 (2012) 311–316, https://doi.org/10.2109/jcersj2.120.311.
[52] K.O. Low, F.R. Sale, Electromagnetic properties of gel-derived NiCuZn ferrites, J. Magn. Magn Mater. 246 (2002) 30–35, https://doi.org/10.1016/S0304-8853(01)01390-7.
[53] H.I. Hsiang, W.C. Kuo, C.S. Hsi, Sintering and cooling atmosphere effects on the microstructure, magnetic properties and DC superposition behavior of NiCuZn ferrites, J. Eur. Ceram. Soc. 37 (2017) 2123–2128, https://doi.org/10.1016/j.jeurceramsoc.2017.01.025.
[54] E. Sánchez, J. García-Ten, A. Barba, V. Beltrán, Estimation of packing density of raw material mixtures used in tile manufacture, Br. Ceram. Trans. 97 (1998) 149–154.
[55] J.S. Reed, Principles of Ceramics Processing, second ed., Wiley, New York, 1995.
[56] W.D. Kingery, H.K. Bowen, D.R. Uhlmann, Introduction to Ceramics, second ed., 1976.
[57] A. Globus, Some physical considerations about the domain wall size theory of magnetization mechanisms, J. Phys. Colloq. 38 (1977), https://doi.org/10.1051/jphyscol:1977101. C1.1-C1.15.
[58] M. Le Floc'h, A.M. Konn, Some of the magnetic properties of polycrystalline soft ferrites: origins and developments of a model for the description of the quasistatic magnetization, J. Phys. IV JP. 7 (1997), https://doi.org/10.1051/jp4:1997169. C1-187-C1-190.
[59] A. Globus, P. Duplex, M. Guyot, Determination of initial magnetization curve from crystallites size and effective anisotropy field, IEEE Trans. Magn. (1971) 617–622, https://doi.org/10.1109/TMAG.1971.1067200.
[60] M.T. Johnson, P.J. Van der Zaag, A. Noordermeer, E.G. Visser, P.T. Por, M. T. Rekveldt, Magnetic permeability and intra-granular domain structure in polycrystalline ferrites, J. Magn. Magn Mater. 104–107 (1992) 421–422, https://doi.org/10.1016/0304-8853(92)90861-H.
[61] P.J. Van Der Zaag, J.J.M. Ruigrok, A. Noordermeer, M.H.W.M. Van Delden, P. T. Por, M.T. Rekveldt, D.M. Donnet, J.N. Chapman, The initial permeability of polycrystalline MnZn ferrites: the influence of domain and microstructure, J. Appl. Phys. 74 (1993) 4085–4095, https://doi.org/10.1063/1.354454.
[62] J. Aarts, I. Abu Shiekah, P.J. Van Der Zaag, Domain structure in polycrystalline MnZn ferrite imaged by magnetic force microscopy, J. Appl. Phys. 85 (1999) 7302–7309, https://doi.org/10.1063/1.369353.
[63] P.J. Van Der Zaag, P.J. Van Der Valk, M.T. Rekveldt, A domain size effect in the magnetic hysteresis of NiZn-ferrites, Appl. Phys. Lett. 69 (1996) 2927–2929, https://doi.org/10.1063/1.117326.

[64] P.J. Van Der Zaag, M. Kolenbrander, M.T. Rekveldt, The effect of intragranular domain walls in MgMnZn-ferrite, J. Appl. Phys. 83 (1998) 6870–6872, https://doi.org/10.1063/1.367562.

[65] J. Bera, P.K. Roy, Effect of grain size on electromagnetic properties of $Ni_{0.7}Zn_{0.3}Fe_2O_4$ ferrite, Phys. B Condens. Matter 363 (2005), https://doi.org/10.1016/j.physb.2005.03.010.

[66] V.D.A.G. Bruggeman, Calculation of various physics constants in heterogenous substances I Dielectricity constants and conductivity of mixed bodies from isotropic substances, Ann. Phys. 24 (1935).